Numerical analysis of Raptor engine's combustion chamber

Corentin Latimier

MECH-6191 : COMBUSTION

Concordia University

Numerical analysis of Raptor engine's combustion chamber

Corentin Latimier[1]

[1]M.Ing. student in Aerospace Engineering, Polytechnique Montréal, Quebec, Canada

Correspondence
Email: corentin.latimier@polymtl.ca

In the present work, SpaceX's Raptor engine combustion chamber has been investigated numerically to precisely understand the flow dynamics and variation of properties such as pressure, temperature and velocity distribution within the combustion chamber. The numerical results were compared to Raptor specifications, demonstrating a strong correspondence. This study shows that improving the correspondence between numerical results and Raptor technical specifications is possible by taking into account the influence of preburners on fuel and oxidizer inlet compositions. In this study, influence of equivalence ratio on engine performance has also been investigated. It has been shown that moving the equivalence ratio from 1.1 to 1.4 can improve engine performance by 5% but it also results in a 5% increase in pressure within the combustion chamber.

KEYWORDS
CFD Analysis, Turbulent non-premixed combustion, Rocket engine, Raptor engine, Numerical simulation, Rocket Nozzle

1 | INTRODUCTION

The utilization of the methane CH_4 and oxygen O_2 propellant combination in rocket engines has gained prominence in contemporary aerospace engineering for multiple reasons. Methane offers a high energetic density, delivering signifi-

Abbreviations: LH_2: liquid hydrogen, GCH_4: gaseous methane, GO_2: gaseous oxygen

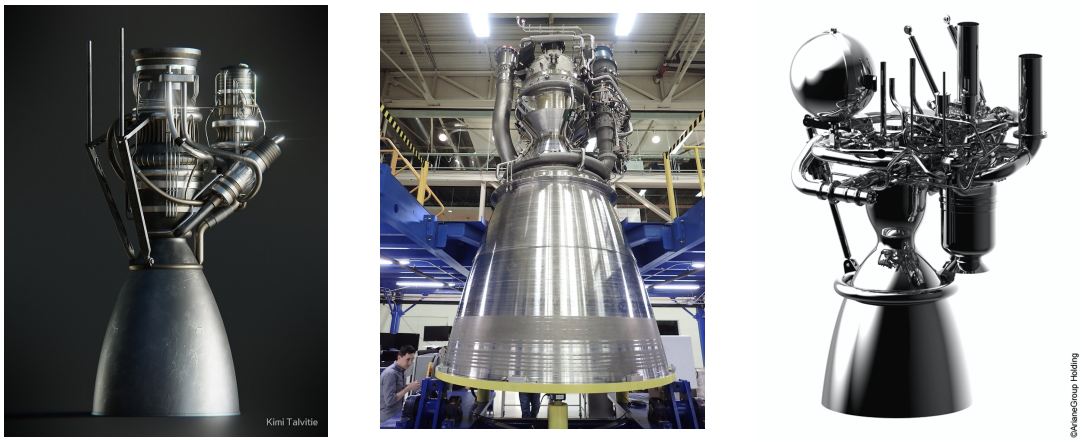

FIGURE 1 From left to right : Raptor (SpaceX), BE-4 (Blue Origin), Prometheus (ArianeGroup)

cant thrust per unit mass. Moreover, it offers the advantage to remain in liquid form at higher temperature compared to other cryogenic fuels (eg. LH2) simplifying the design and operation of storage systems. In the context of a growing interest for reusable launchers, the adoption of CH_4/LO_x configurations is suitable because of it's lower combustion temperature and reduced wear and tear on engine components. Finally, considering future space exploration and colonization, methane offers the advantage of being able to be produced in-situ in space using local resources such as CO_2 extracted from the martian atmosphere and hydrogen from water. These are some of the main reasons that explain why CH_4/LO_x rocket engines are today considered as one of the most promising configurations and justify it's adoption by major space actors such as SpaceX (Raptor), Blue Origin (BE-4), ArianeGroup (Prometheus), etc.

In a rocket engine, the propellant is injected into the combustion chamber and burn at very high temperature. The rocket engine nozzle, generally a convergent-divergent type, converts the heat generated by combustion of fuel and oxidizer into kinetic energy. The slowly moving, high pressure and high temperature gases are converted into low pressure, low temperature and high speed gases by the nozzle, generating thrust. Exit gases are generally supersonic. The design and the optimization of a rocket engine must be lead by a deep understanding of these phenomena occurring during combustion process. Three different kind of physics are crucial to consider in numerical simulations so as to obtain numerical results showing good agreements with experimental ones : combustion, fluid dynamics and heat transfer. Numerical simulations of rocket engine's combustion are thus highly multi physics. In this regard, this work aims to establish a methodology to simulate with fidelity GCH_4/GO_2 combustion in rocket engines. To confirm good agreements with experimental results, numerical results are compared with SpaceX's Raptor engine performances. Then, effects of combustion parameters and combustion chamber design are investigated numerically.

2 | RAPTOR ENGINE PRESENTATION

Raptor engine is a family of full-staged-combustion-cycle rocket engine developed and used by SpaceX for use on the SpaceX Starship. The present work focuses on the Raptor sea level variant. The engine is powered by cryogenic liquid methane and liquid oxygen in a full-staged-combustion-cycle: an oxygen-rich turbine powers an oxygen turbopump, and fuel-rich turbine powers a methane turbopump. Both streams —oxidizer and fuel- are then mixed completely in

the gas phase before they combust.

2.1 | Raptor technical information

The main technical information used in the project are presented in the table below.

TABLE 1 Raptor sea level technical information (dimensions, propellant, performances, design features)

Dimensions		**Source**
Nozzle exit diameter	1.3 m	SpaceX [1]
Throat to exit length	1.5 m	SpaceX [1]
Area Ratio	40	Federal Aviation Administration (FAA) [2]
Propellant		**Source**
O/F	3.6	Wikipedia [3]
GCH_4 inlet temperature	800 K	Wikipedia [3]
GO_2 inlet temperature	700 K	Wikipedia [3]
Fuel mass flow	140 kg/s	Wikipedia [3]
Oxidizer mass flow	510 kg/s	Wikipedia [3]
Performances		**Source**
ISP	327 s	Wikipedia [3]
Thrust	2.3 MN	Wikipedia [3]
Chamber pressure	300 bar (nominal)	Wikipedia [3]
Design features		**Source**
Cooling technique	Regenerative cooling	SpaceX [1]
Injector design	Coaxial swirl injectors	Wikipedia [3]

OF: Oxidizer to Fuel ratio; ISP : Specific impulse.

If needed, additional and more specific information will be presented in the next sections.

3 | METHODOLOGY

The objective of this study is to conduct a numerical investigation into the physical phenomena within the combustion chamber of the Raptor engine, with the overarching goals of optimizing its design and enhancing comprehension of the design principles employed by SpaceX. For this purpose, a computational model integrating a 2D axisymmetric convergent-divergent nozzle with a combustion chamber is developed. An initial simulation is undertaken to assess the fidelity of the model by comparing numerical results with empirical test data, thereby validating its accuracy. Then, once validity of the model is verified, numerical investigations are conducted to understand the influence of various parameters on the overall performance of the engine. These simulations are carried out using ANSYS fluent.

3.1 | Procedure of analysis

3.1.1 | Geometry

The nozzle geometry was created using the method of characteristics based on technical information shown in Table 3. The nozzle's profile was exported in ANSYS design modeler. The injector plate of the Raptor engine comprises 640

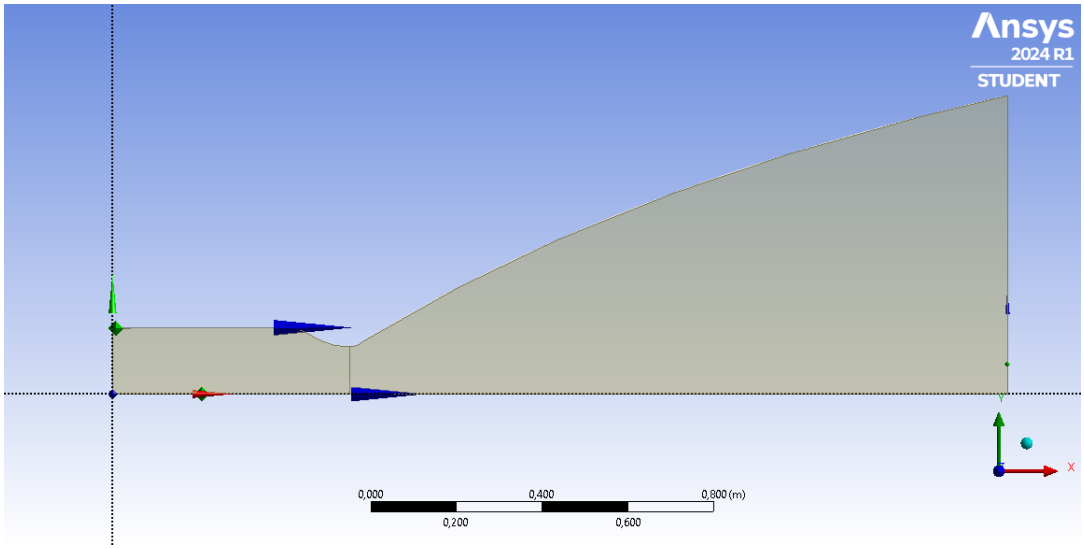

FIGURE 2 Raptor Sea Level design in ANSYS Modeler

injectors coaxial swirl injectors distributed evenly across its surface. These injectors are arranged in a radial pattern, with 20 injectors spanning the diameter of the injector plate. Considering the 2D-axisymmetric nature of our model, we have accordingly subdivided the combustion chamber inlet into 10 injectors. In this work, each injector is separated from the other with a distance E and has a diameter $D_{injector}$.

The Raptor engine is equipped of **coaxial swirl injectors**. A coaxial swirl injector is designed to mix fuel and oxidizer efficiently before combustion. It consists of two concentric passages. The central passage serves to impart swirling motion to the fuel, while the outer passage directs the oxidizer stream in a linear trajectory providing an efficient mixing. The diameter of central passage is $D_{central}$.

TABLE 2 Key dimensions of the injector plate in the CFD model

Dimensions	
E	5 mm
$D_{injector}$	10 mm
$D_{central}$	2 mm

3.1.2 | Meshing

The geometry is discretized by generating a fully structured quadrilateral mesh. Proper care is taken while meshing regions near the nozzle and the combustion chamber wall to get more refinment so as to calculate with precision the steep gradients of velocity components due to viscous effects. Mesh is refined near the injectors so as to simulate with precision the mixing between oxidizer and fuel. The region near the throat of the nozzle is also refined. The final mesh is composed of 108540 cells.

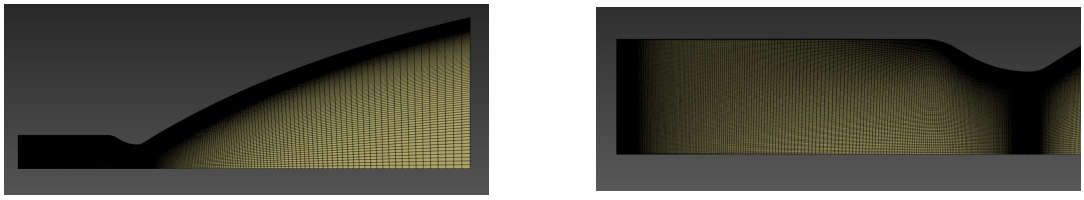

FIGURE 3 Mesh overview - Overall mesh (left) and detail of the meshing of the combustion chamber (right)

3.1.3 | Boundary conditions

In order to accurately model combustion, it is essential to address four fundamental conservation equations: **mass**, **momentum**, **energy**, and **species mass** conservation. Properly configuring the numerical problem necessitates imposing appropriate boundary conditions for each of these equations. The boundary conditions used in the model for the initial simulation are presented below.

Oxidizer and fuel inlets

The boundary conditions for the oxidizer and fuel inlets are defined as mass flow inlets based on the specifications provided in Table 3, resulting in an oxidizer-to-fuel (O/F) ratio of 3.6. Inlet turbulent intensity is fixed to 10% for fuel inlets to represent turbulence due to the swirling motion and 5% for oxidizer inlets. Inlet temperatures for both fuel and oxidizer are determined in accordance with Table 3. In an initial approximation, the mass fractions of fuel and oxidizer at the inlet are assumed to be unity, although in reality, this may not hold true as the Raptor engine operates on a full staged combustion cycle. This point will be investigated in the next sections.

Outlet

The outlet boundary condition is specified as a pressure outlet. The outlet pressure is set to 0 Pa.

Walls

A no-slip boundary condition is applied to the walls. In the initial approach, the walls are treated as adiabatic, resulting in a zero heat flux through them. Chamber walls are also considered non reactive.

Axis

An axis boundary condition is applied to the axis of the engine.

3.1.4 | Governing equations

The mathematical modeling relies on steady-state continuity, momentum, energy, and species conservation equations. Given the highly turbulent nature of the flow in the combustion chamber and nozzle, the Reynolds-Averaged Navier-Stokes (RANS) approach is employed. The gravitational force is neglected. As heat is liberated during the combustion process, it induces substantial local temperature elevations, rendering the flow compressible. To take into account these compressible effects, *Favre Averaging Navier-Stokes* equations are used. The combustion is modelled using non adiabatic non-premixed combustion model. *Note : Considering a variable y, the time averaged value of y is denoted as $\bar{y}$ and the density-weighted average of y is denoted as $\tilde{y}$*

Continuity equation

$$\frac{\partial(\bar{\rho}\tilde{u}_i)}{\partial x_i} = 0$$

Momentum conservation : i-direction

$$\frac{\partial(\bar{\rho}\tilde{u}_i\tilde{u}_j)}{\partial x_j} = -\frac{\partial\bar{p}}{\partial x_i} + \frac{\partial}{\partial x_j}(\mu\frac{\partial\tilde{u}_i}{\partial x_j}) - \frac{\partial}{\partial x_j}(\overline{\rho u_i'' u_j''})$$

The Reynolds stress i.e : $\frac{\partial}{\partial x_j}\overline{\rho u_i'' u_j''}$ is *modelled* using the $k\omega$-SST model leading to equation :

$$\frac{\partial(\bar{\rho}\tilde{u}_i\tilde{u}_j)}{\partial x_j} = -\frac{\partial}{\partial x_i}(\bar{p} + \frac{2}{3}\bar{\rho}\bar{k}) + \frac{\partial}{\partial x_j}((\mu + \mu_t)\frac{\partial\tilde{u}_i}{\partial x_j})$$

with $\bar{k}$ the turbulent kinetic energy and μ_t the eddy viscosity. These two additional quantities are solved with two additional transport equations, specific to the $k\omega$-SST turbulence model.

Energy equation

The energy equation used in the model is based on the assumption that the Lewis number L_e is unity.

$$\vec{\nabla}\cdot(\bar{\rho}\vec{\tilde{v}}\tilde{H}) = \vec{\nabla}\cdot(\frac{k_t}{C_p}\vec{\nabla}(\tilde{H})) + \bar{S_h}$$

where H is the total enthalpy of the mixture, k_t the turbulent thermal conductivity (defined according the $k\omega$-SST model) and S_h is the contribution from viscous dissipation. The mixture total enthalpy is defined as :

$$H = \sum_j Y_j H_j$$

with Y_j the mass fraction of species j and

$$H_j = h_j^0(T_ref) + \int_{T_{ref}}^{T} Cp_j dT$$

$h_j^0(T_{ref})$ is the formation enthalpy of species j at the reference temperature T_{ref}.

The source of energy due to chemical reactions is included in the definition of enthalpy with the heat of formation of species. The effect of enthalpy transport due to species diffusion does not explicitely appear in the energy equation because it is included in the first term of the right hand side of equation.

Species conservation equations

$$\vec{\nabla} \cdot (\bar{\rho}\vec{\tilde{v}}\tilde{Y}_j) = -\vec{\nabla} \cdot \vec{J}_j + \bar{R}_j$$

where Y_j is the mass fraction of species j, R_j is the net rate of production of species j by chemical reactions and $\vec{J}_j$ is the diffusion flux of species j.

In turbulent flows, Ansys Fluent computes the mass diffusion in the following form :

$$\vec{J}_j = -(\rho D_{j,m} + \frac{\mu_t}{S_{ct}})\vec{\nabla}(Y_j) - D_{T,j}\frac{\vec{\nabla}(T)}{T}$$

where $D_{j,m}$ is the mass diffusion coefficient for species j in the mixture, $D_{T,j}$ is the thermal (Soret) diffusion coefficient and S_{ct} is the turbulent Schmidt number ($\frac{\mu_t}{\rho D_t}$ where μ_t is the turbulent viscosity and D_t is the turbulent diffusivity).

3.1.5 | Combustion modelling

The equations presented before involve density-weighted average quantities (denoted with ˜ symbol). To calculate these quantities, the **probability density function** (PDF) approach is used. In combustion modeling, the probability density function (PDF) is a mathematical tool used to describe the statistical distribution of certain properties within a combustion system. The idea behind using PDFs in combustion modeling is to represent how key variables, such as temperature, species concentrations, and reaction rates, are distributed across a range of values within the combustion system. This distribution provides insights into the variations and fluctuations that occur due to factors like turbulence, mixing, and chemical kinetics. In this work, the model is coupled with a presumed PDF (beta PDF) to describe the probability distribution of the mixture fraction, which represents the local composition of the mixture in the combustion chamber.

Using the assumed PDF function $P(\xi)$, we can calculate key quantities such as density-weighted average of the mass fraction of species i as :

$$\tilde{Y}_i = \int_0^1 Y_i(\xi)\tilde{P}(\xi)d\xi \text{ with } \tilde{P}(\xi) = \frac{\rho(\xi)}{\bar{\rho}}P(\xi)$$

3.1.6 | Chemical kinetics

The chemical kinetics of the CFD-model are extracted from **GRI-Mech** chemical kinetics database [4].GRI-Mech is a list of elementary chemical reactions and associated rate constant expressions. It contains 53 species and 325 reactions. GRI-Mech was used because the database is optimized for methane as a fuel. The reaction rate coefficient

obeys to the Arrhenius law:

$$k_f = AT^n \exp -\frac{E_a}{T}$$

where A is the pre-exponential factor, E_a is the activation energy, T the temperature and n is the temperature exponent.

3.1.7 | Thermochemistry properties

The thermochemistry properties of each species are extracted from the database associated with the GRI-Mech database.

3.1.8 | Solver settings and convergence of the solution

The solution method used is the **SIMPLE** algorithm (Semi Implicit Method for Pressure Linked Equations). The convergence of the solution is estimated by mathematical residuals that need to be minimal and key parameters of the rocket engine that need to be constant for fully converged solution :

- Mass flux at the outlet
- Averaged axial velocity at the outlet
- Averaged temperature at the throat of the nozzle

4 | RESULTS AND DISCUSSIONS - INITIAL SIMULATION

4.1 | Convergence analysis

The solution is converged for **456** iterations according to the criterions defined above.

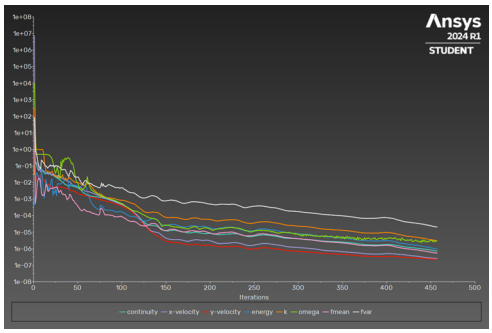

FIGURE 4 Evolution of normalized residuals through iterations

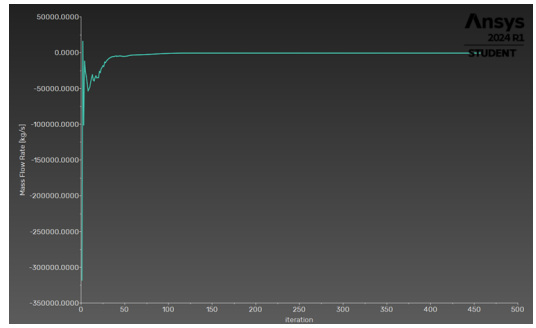

FIGURE 5 Evolution of mass flux through iterations

Mass flux at outlet of the nozzle converges to the constant value of $\dot{m}_{outlet} = -650$ kg/s. This value is negative because the mass exits the computational domain. The conservation of mass is respected because $\dot{m}_{fuel} + \dot{m}_{oxidizer} = 650$

kg/s.

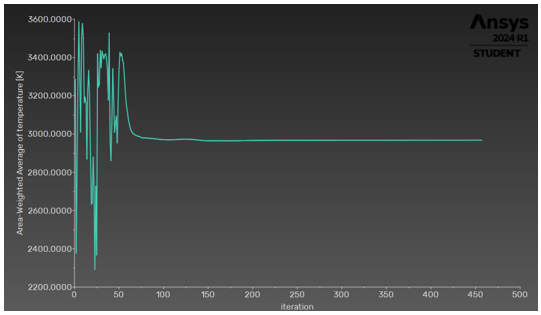

FIGURE 6 Evolution of averaged temperature at the throat section of the nozzle through iterations

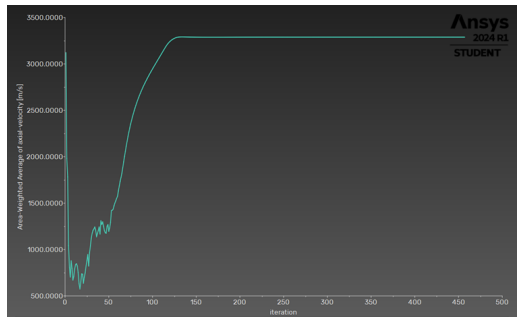

FIGURE 7 Evolution of averaged velocity at the nozzle outlet through iterations

The averaged temperature at the throat section converges to T_{av}^{throat} = 2966K. The averaged velocity at the nozzle outlet converges to V_{av}^{outlet} = 3288 m/s which corresponds to a Mach number of 4.

4.2 | Pressure

When fuel and oxidizer enter the combustion chamber, they mix and burn due to high speed and high temperature. This combustion process leads to an increase in pressure within the chamber. In the combustion chamber, the combustion gases experience a small pressure drop. When the gases enter the convergent-divergent nozzle, pressure is converted into kinetic energy and there is consequently an high pressure drop. The distribution of pressure in the rocket engine is presented below.

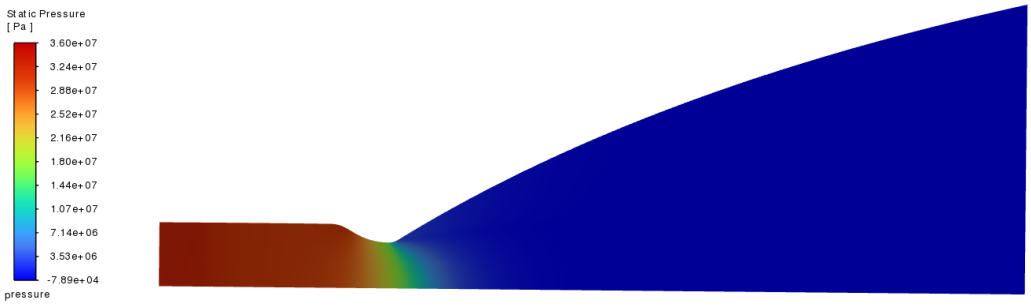

FIGURE 8 Pressure distribution in the rocket engine - Initial simulation

The evolution of pressure along the axis of the combustion chamber is shown below.

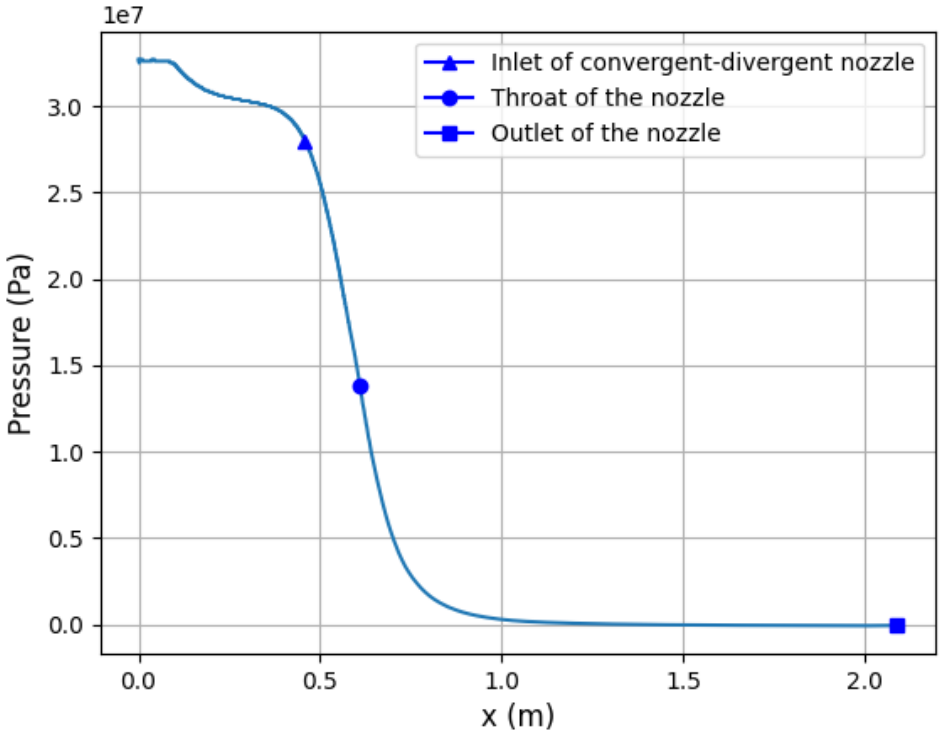

FIGURE 9 Evolution of pressure along axis - Initial simulation

The average pressure within the combustion chamber measures 317.4 bar. As outlined in the technical specifications of the Raptor engine (refer to Table 3), the expected pressure within the chamber stands at 300 bar. Hence, our simulation closely aligns with the provided technical data, demonstrating a difference of 6% in pressure.

4.3 | Temperature

After combustion, the temperature rises instantaneously in the combustion chamber. After entering the convergent-divergent nozzle, internal energy of the combustion gases is converted into kinetic energy. There is consequently an high temperature drop. The distribution of temperature in the nozzle is presented below.

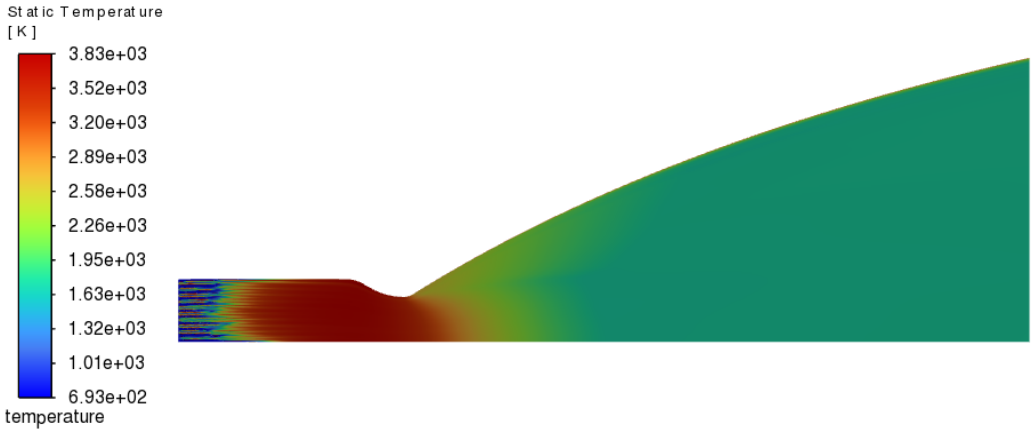

FIGURE 10 Distribution of temperature - Initial simulation

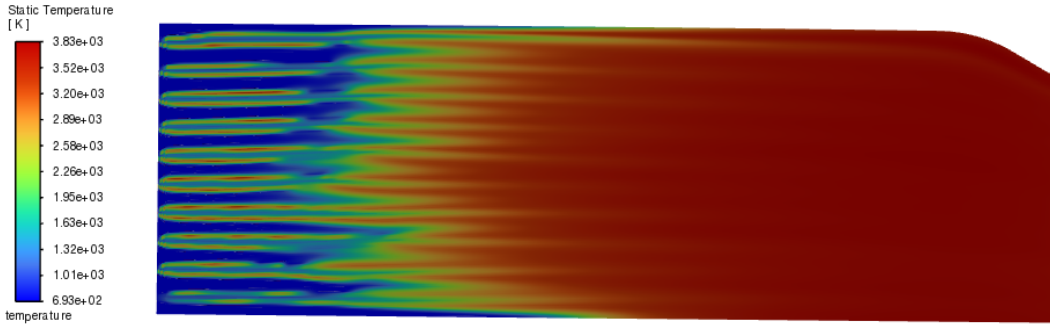

FIGURE 11 Distribution of temperature : zoom on the inlet - Initial simulation

The combustion process between GCH_4 and GO_2 is evident in Figure 11. A notable increase in temperature is observed, indicating combustion occurring slightly before the midpoint of the combustion chamber. The combustion chamber reaches a peak temperature of 3830 K. Using Cantera for validation confirms that this temperature aligns

closely with theoretical predictions. Adhering to adiabatic conditions at constant pressure (which is the case in the model, refer to previous section), the computed adiabatic flame temperature stands at 3955 K. This temperature is far from reality since walls of the rocket engine are considered as adiabatic in the model. In reality, cooling techniques are used to avoid walls from melting, which reduce gas temperature. The evolution of pressure along the axis of the combustion chamber is shown below.

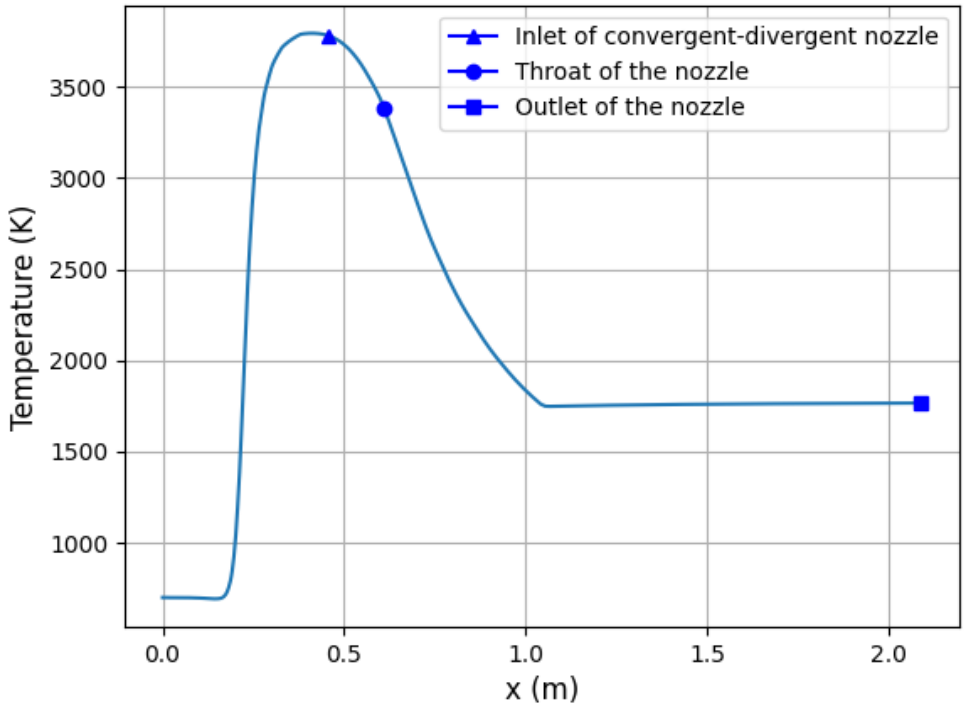

FIGURE 12 Evolution of temperature along axis - Initial Simulation

4.4 | Velocity

As the combustion products progress through the rocket engine, their velocity increases while pressure and temperature concurrently decreases. The evolution of axial velocity along the axis of the rocket engine is shown below. The velocity increases as the gases moves forward in the rocket engine. There are some fluctuations of the axial velocity in the combustion chamber due to the combustion process. The gas velocity at nozzle exit is 3288.4 m/s, which corresponds to a specific impulse of 335 s. In comparison, the technical specifications of the Raptor engine (refer to Table 3) stipulate a specific impulse of 327s. Consequently, our numerical model exhibits a deviation of 2.4% in ISP estimation, indicating a relatively precise approximation.

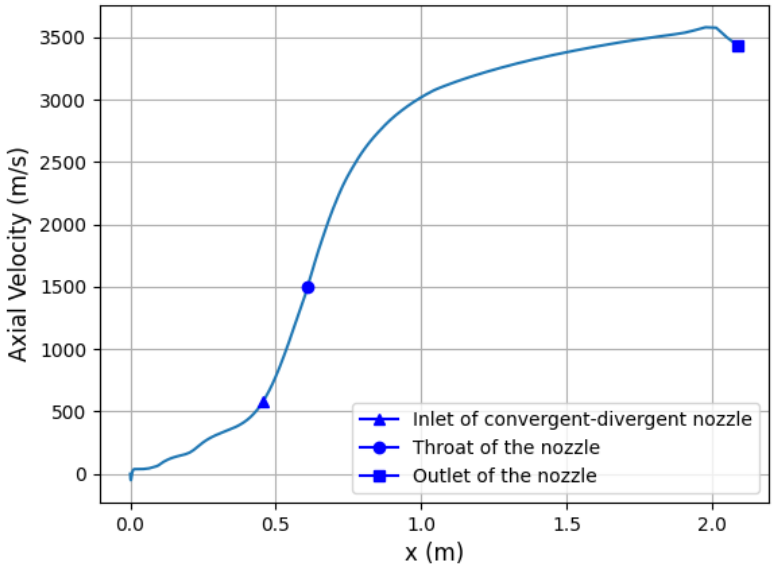

FIGURE 13 Evolution of axial velocity u along axis - Initial Simulation

To validate rocket engine design constructed using the method of characteristics, Mach number (M_a) distribution within the rocket engine is analysed. An optimal design should yield a M_a value of 1 at the throat, indicating a transition from subsonic flow in the convergent portion to supersonic flow in the divergent section of the nozzle. The distribution of Mach number in the rocket engine is shown below.

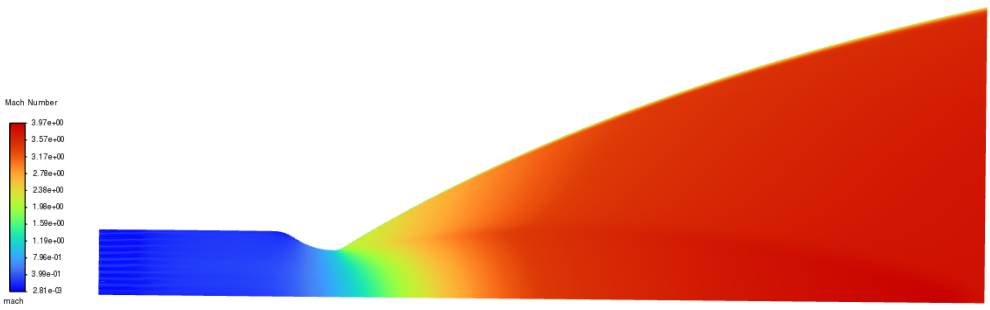

FIGURE 14 Distribution of Mach number - Initial Simulation

The evolution of Mach number along the axis of the rocket engine is shown below.

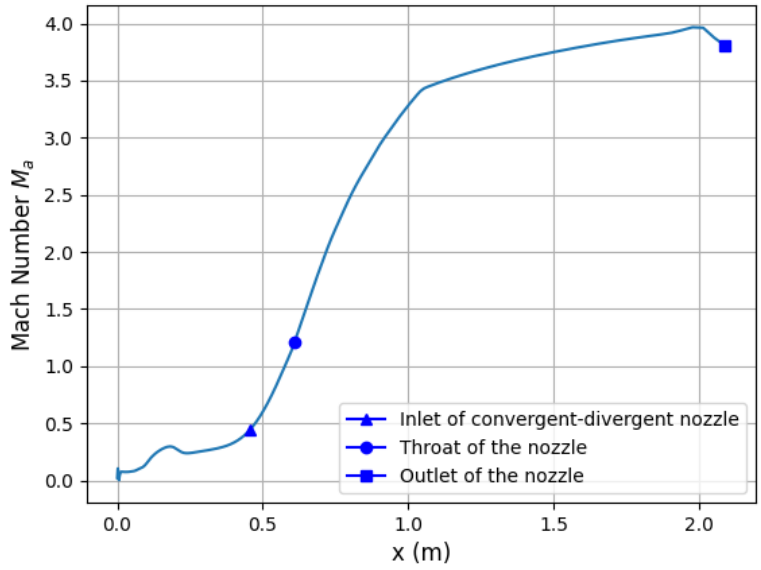

FIGURE 15 Evolution of Mach number along axis - Initial Simulation

Examination reveals that the flow transitions to supersonic conditions just before the throat. At the throat itself, the Mach number is 1.2. Therefore, the rocket engine design fits the flow conditions effectively. At the outlet, the flow exits at a Mach number of 3.8.

4.5 | Species mass fractions

4.5.1 | Reactants mass fractions

The distribution of mass fractions of $CH4$ and $O2$ are shown below.

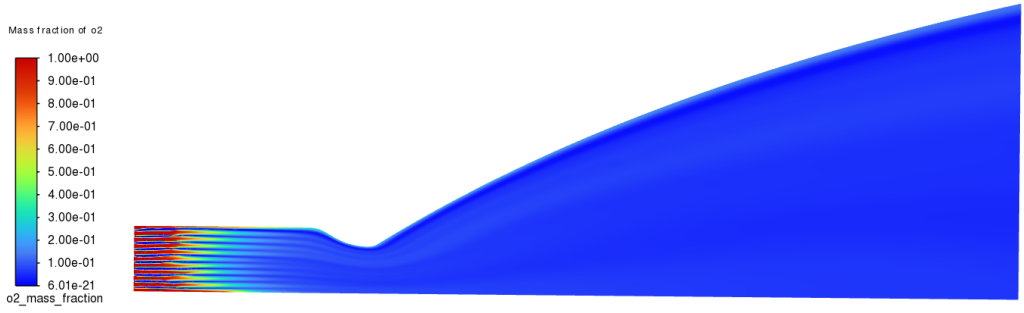

FIGURE 16 Distribution of $O2$ mass fraction (Y_{02}) - Initial Simulation

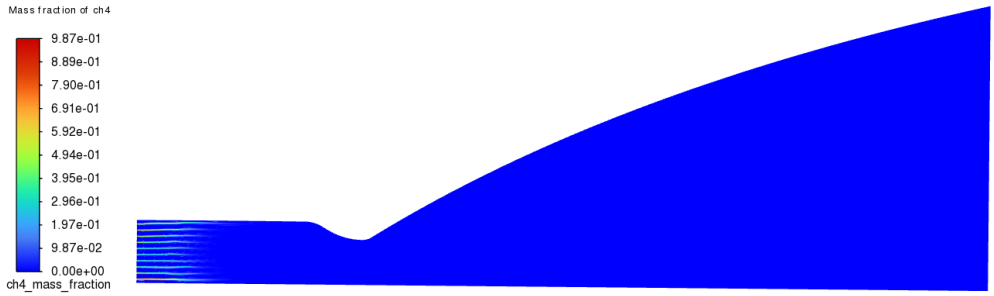

FIGURE 17 Distribution of CH_4 mass fraction (Y_{CH_4}) - Initial Simulation

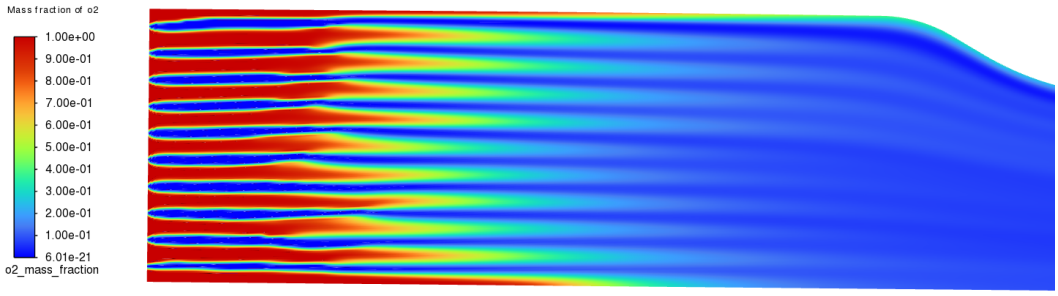

FIGURE 18 Distribution of O_2 mass fraction (Y_{O_2}) : Zoom on the inlet - Initial Simulation

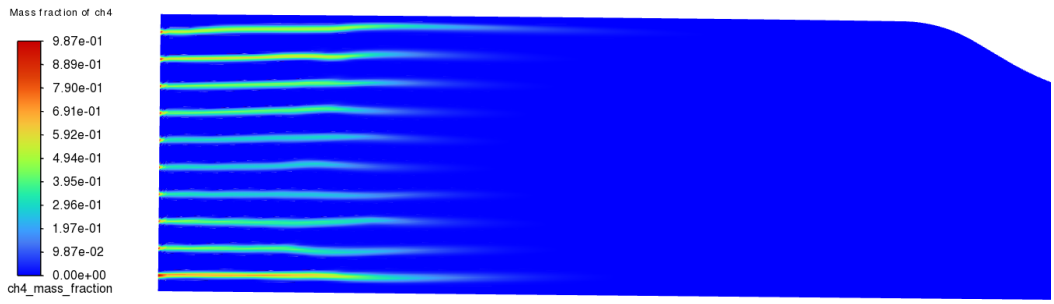

FIGURE 19 Distribution of CH_4 mass fraction (Y_{CH_4}) : Zoom on the inlet - Initial Simulation

The negligible presence of CH_4 and O_2 in the downstream of the combustion chamber suggests effective combustion

of the propellants. Using Figure 19, we can estimate the flame length which is approximately 11 cm. In Figure 18, a small amount of unburnt O_2 is observable within the shear layer of the rocket engine. Figure 16 illustrates that there remains some O_2 at the outlet, while the presence of CH_4 is negligible. This observation is further supported by the figure below, depicting the mass fraction of CH_4 and O_2 at the outlet.

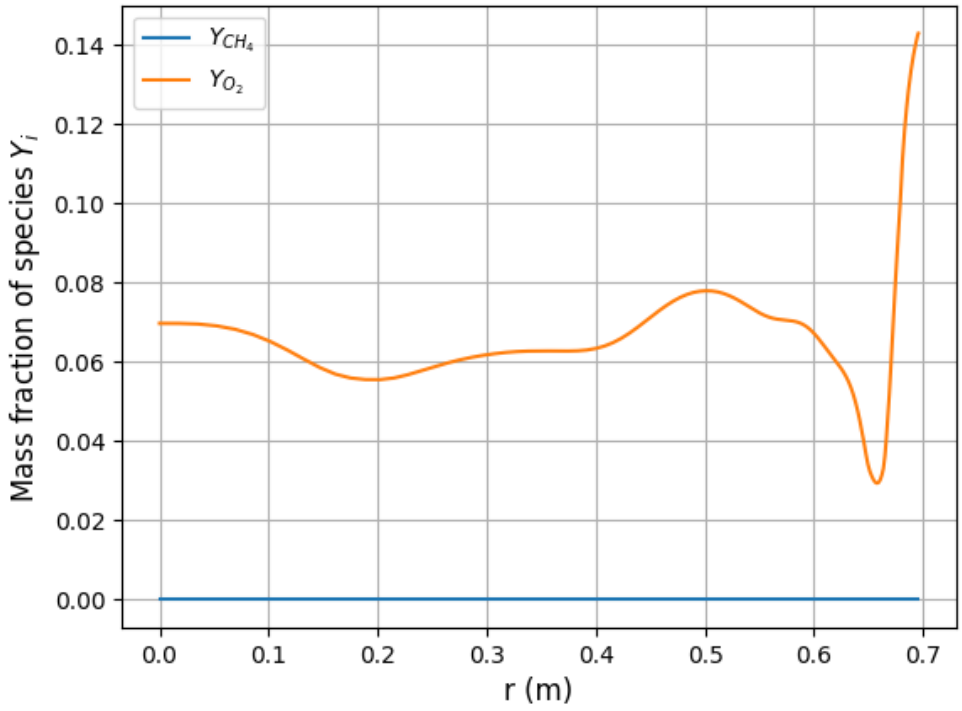

FIGURE 20 Distribution of CH_4 mass fraction (Y_{CH_4}) and O_2 mass fraction (Y_{O_2}) at the outlet - Initial Simulation

There is no CH_4 at the outlet, there is still O_2. Particularly, there's a noticeable peak close to the nozzle wall, which comes from the unburnt O_2 in the nozzle's shear layer. This observation is unexpected because the Raptor engine's combustion is fuel rich ($\phi = 1.1$). This phenomenon is believed to occur due to the high temperatures in the combustion chamber, causing the thermal decomposition of CH_4. As a result, CH_4 cannot react completely with all the supplied O_2, leaving some O_2 unburnt at the exit.

4.5.2 | Products mass fractions

The major products of CH_4/O_2 combustion are CO_2 and H_2O. Additionally, a notable presence of carbon monoxide (CO) is observed among the secondary product species, due to the thermal decomposition of CO_2 at high temperatures. The spatial distributions of these products within the rocket engine are illustrated in the figures below.

FIGURE 21 Distribution of CO_2 mass fraction (Y_{CO_2}) - Initial Simulation

FIGURE 22 Distribution of H_2O mass fraction (Y_{H_2O}) - Initial Simulation

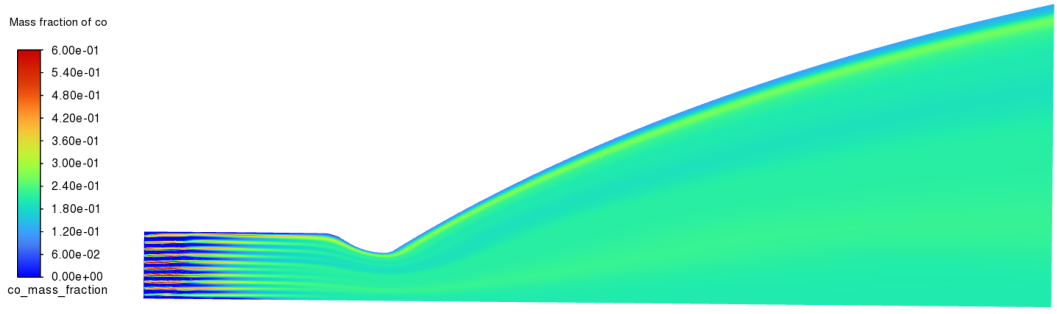

FIGURE 23 Distribution of CO mass fraction (Y_{CO}) - Initial Simulation

There is an high concentration of carbon monoxide (CO) in close proximity to the nozzle wall, as depicted in Figure 23. This occurrence aligns with regions characterized by diminished mass fractions of carbon dioxide (CO_2) (refer to Figure 21). This observation suggests that carbon dioxide dissociates into carbon monoxide along these particular streamlines. The distribution of $C0_2$ and CO mass fraction at outlet is shown in the figure below.

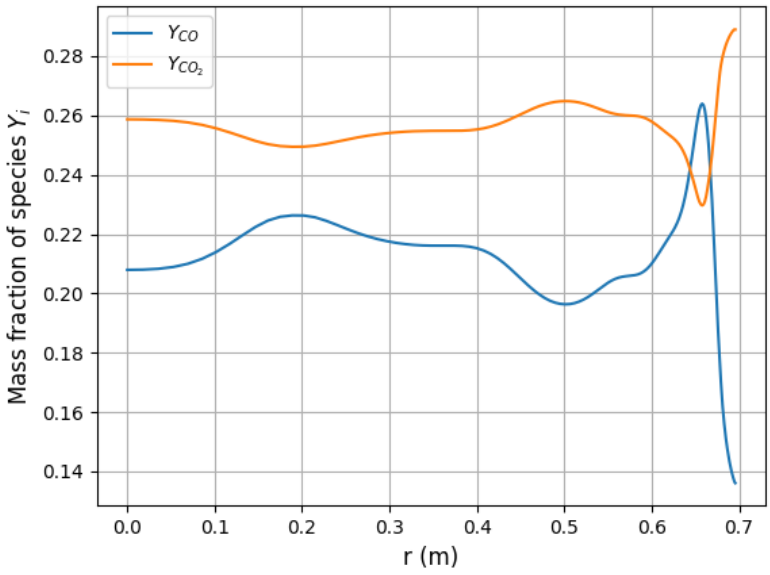

FIGURE 24 Distribution of CO and CO_2 mass fraction - Initial Simulation

Examining Figure 24, we notice a rise in the mass fraction of carbon monoxide (CO) at points where the mass fraction of carbon dioxide (CO_2) decreases near the nozzle wall. This observation supports our initial hypothesis.

The mass fractions of species at the nozzle exit are shown below and are compared with Cantera calculation for validation.

Species	Mass fraction at outlet (Fluent)	Mass fraction (Cantera)
H_20	**0.381**	0.387
CO_2	**0.257**	0.257
CO	**0.211**	0.217
O_2	**0.067**	0.0546
OH	**0.0642**	0.0655
O	**0.0111**	0.0108
H_2	**0.0065**	0.0065
H	**0.00098**	0.0010172

Mass fraction of species at nozzle outlet shows good agreement with Cantera calculation.

4.6 | Comparison of numerical results with Raptor engine specifications

A comparison of the numerical results from the initial simulation with the specifications of the Raptor engine is shown below.

	Numerical results	Raptor engine Specs	Deviation (%)
Specific Impulse (s)	335	327	**+2.4**
Thrust (MN)	2.14	2.3	**-7.1**
Chamber mean pressure (bar)	317.4	300	**+5.8**
Max. temperature in combustion chamber (K)	3830	3700	**+3.5**

The initial simulation demonstrates a good level of accuracy when compared with the specifications of the Raptor engine. Consequently, this affirms the validity and robustness of the methodology employed for modeling combustion within the rocket engine. Consequently, the same methodology is employed to investigate the impact of some combustion and design parameters on the performance of the Raptor engine.

5 | ANALYSIS OF THE IMPACT OF COMBUSTION PARAMETERS ON ROCKET ENGINE PERFORMANCE

In this section, the influence of various combustion parameters on the performance of the Raptor engine is analysed, using the validated numerical model from the initial simulation. Specifically, the following combustion parameters are investigated:

- Influence of LOX and $CH4$ preburners
- Influence of equivalence ratio Φ

5.1 | Influence of LOX and $CH4$ preburners

To transport propellants from the tanks to the combustion chamber and to pressurize them, the Raptor engine utilizes two pumps : a methane turbopump and a LOX turbopump. These pumps are driven by turbines powered by a portion of the propellant flow. These turbines extract energy from the flow of propellants and use it to drive the pumps, providing a self-sustaining propulsion system with high efficiency and power density.

Raptor engine is a full-flow staged combustion (FFSC) engine. It is a twin-shaft staged combustion cycle that uses both oxidizer-rich and fuel-rich preburners to give energy to the turbines. This cycle permits the full flow of both propellants through the turbines; hence the name. The fuel turbopump is driven by the fuel-rich preburner, and the oxidizer turbopump is driven by the oxidizer-rich preburner. Due to this configuration, the propellants do not directly enter the main combustion chamber as pure methane and oxygen. Instead, they are delivered as methane-rich and oxygen-rich gases, originating from the methane preburner and oxygen preburner, respectively. The Raptor engine

cyle diagram is shown below.

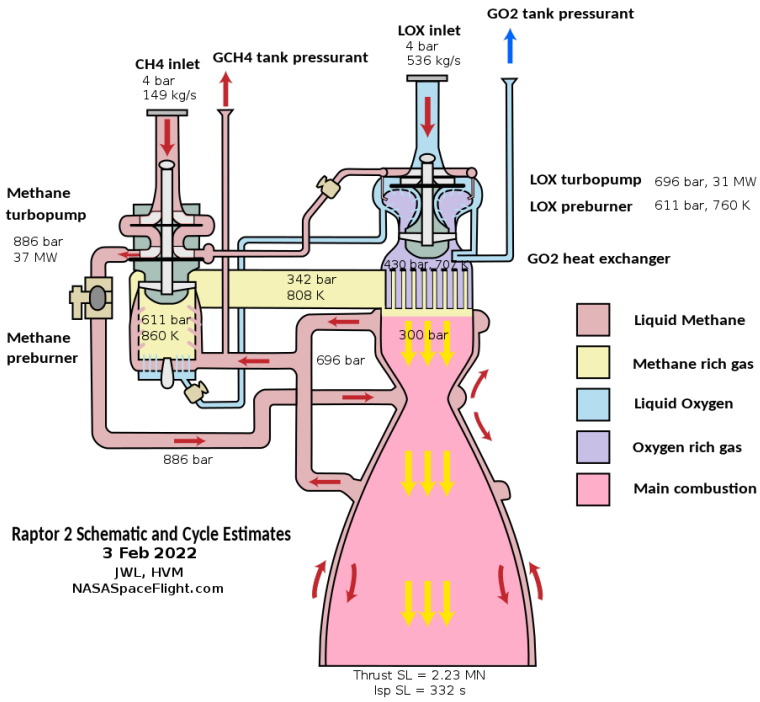

FIGURE 25 Raptor engine cycle diagram with estimates from open-source information and analysis

In the initial simulation, the assumption was that the fuel and oxidizer entering the main combustion chamber would be pure methane and oxygen. However, the presence of preburners modifies the composition of the fuel and oxidizer inlets to the main combustion chamber. Consequently, this modification has an impact on the performance of the engine. This section aims to assess and quantify the impact of these compositional changes on engine performance.

Cantera calculations have been found to present good agreement with Ansys Fluent in estimating species mass fractions after combustion. Consequently, instead of using Ansys Fluent to simulate combustion in the LOX and CH4 preburners to calculate the composition of the fuel and oxidizer inlets for the main combustion chamber, Cantera is employed for this purpose.

The essential informations regarding the CH4 and LOX preburners are provided below.

TABLE 3 Key informations about $CH4$ and LOX preburners [5]

	CH4 preburner	LOX preburner
Φ (Equivalence Ratio)	24.5	0.058
Reactants inlet temperature	280 K	90 K
Pressure	611 bar	696 bar

Methane preburner is fuel-rich, while the oxygen preburner is fuel-lean. Also, the oxygen enters the LOX preburner as a liquid, at cryogenic temperature.

Using Cantera, the product species at the exit of the preburners are determined and subsequently employed to specify the composition of the fuel and oxidizer at the inlet of the main combustion chamber. The table below presents the composition (in terms of mass fraction) of the fuel and oxidizer at the inlet of the main combustion chamber, taking into account the preburners.

Species	Fuel inlet (*Methane preburner outlet*)	Oxidizer inlet (*LOX preburner outlet*)
CH_4	0.816	0
O_2	0	0.928
CO_2	0.10	0.04
H_20	0.07	0.032
CO	0.008	0
H_2	0.003	0
C_2H_6	0.003	0

The preburners lead to a small pressure drop within the combustion chamber, reducing from 317 bar without preburners to 300 bar (-5%). The maximum temperature within the combustion chamber also decreases, from 3830 K to 3650 K, representing a reduction of 4.7%. The gas velocity at the nozzle exit is 3242 m/s, yielding a specific impulse of 330 s, which signifies a decrease of 1.5% compared to the configuration without preburners.

The comparison of the numerical results obtained from the simulation **with preburners** with the specifications of the Raptor engine is shown:

	Numerical results	Raptor engine Specs	Deviation (%)
Specific Impulse (s)	330	327	**+0.9**
Chamber mean pressure (bar)	300	300	**0**
Max. temperature in combustion chamber (K)	3650	3700	**+1.4**

Considering preburners results in a higher level of accuracy compared to the specifications of the Raptor engine.

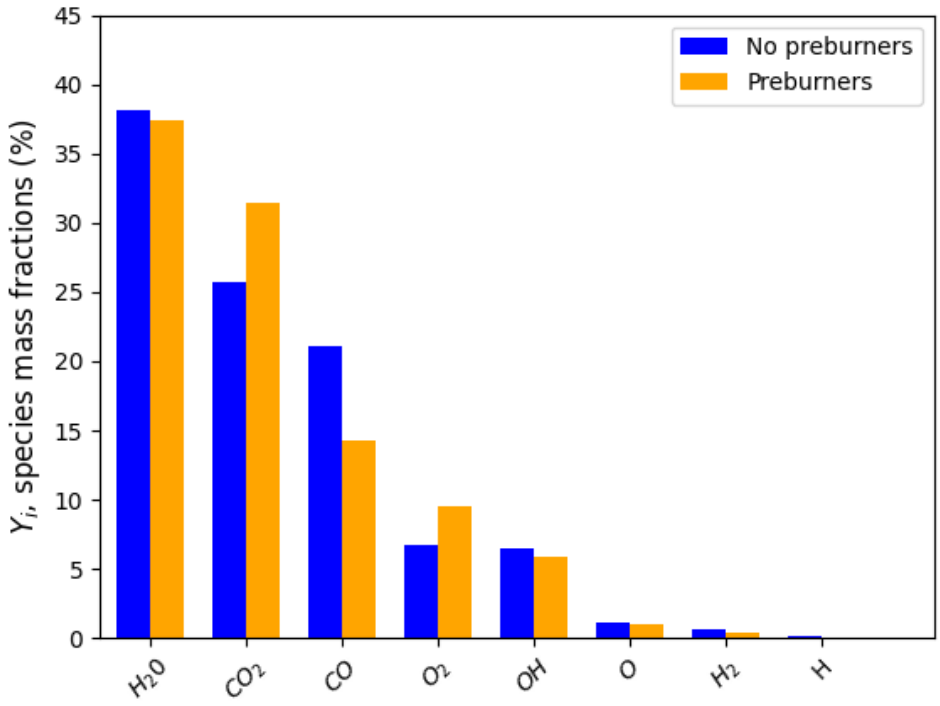

FIGURE 26 Comparison of species mass fraction at nozzle exit: rocket engine with pure CH_4/O_2 vs. rocket engine with preburners

The presence of preburners increases the concentrations of CO2 at the nozzle exit and diminishes the presence of CO, suggesting less CO2 thermal decomposition inside the engine.

5.2 | Influence of equivalence ratio Φ

In this section, the effect of equivalence ratio on Raptor performance is investigated. The oxidizer and fuel inlet temperatures are kept constant from the previous section. The total mass flow rate through the engine is maintained at a constant value of $\dot{m} = 650$ kg/s. Preburners are not considered to simplify the analysis.

The global stoichiometric reaction of CH_4/O_2 combustion is given by :

$$CH_4 + 2O_2 \rightarrow CO_2 + 2H_20$$

Consequently, the stoichiometric oxidizer-to-fuel ratio is determined by:

$$(O/F)_{stoich} = \frac{2MW_{O_2}}{MW_{CH_4}} = 4$$

At its operational nominal point, the engine exhibits an (O/F) ratio of $(O/F) = \frac{\dot{m}O_2}{\dot{m}CH_4} = 3.64$, resulting in an equivalence ratio Φ_{nom} of 1.11. At this operational point, the Raptor engine operates within a fuel-rich regime, close to the stoichiometric mixture. To examine the impact of equivalence ratio on engine performance, calculations are carried out across the range from Φ = 0.5 to Φ = 2.6. Results are shown in the figures below.

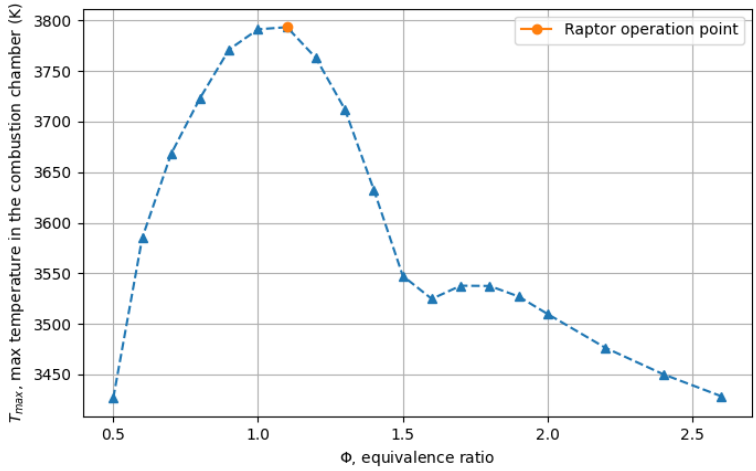

FIGURE 27 Evolution of maximum temperature within the combustion chamber versus equivalence ratio Φ

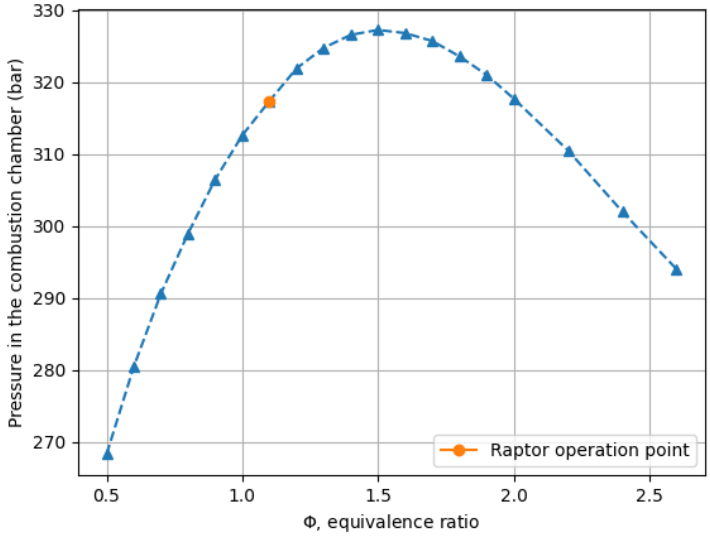

FIGURE 28 Evolution of mean pressure in the combustion chamber versus equivalence ratio Φ

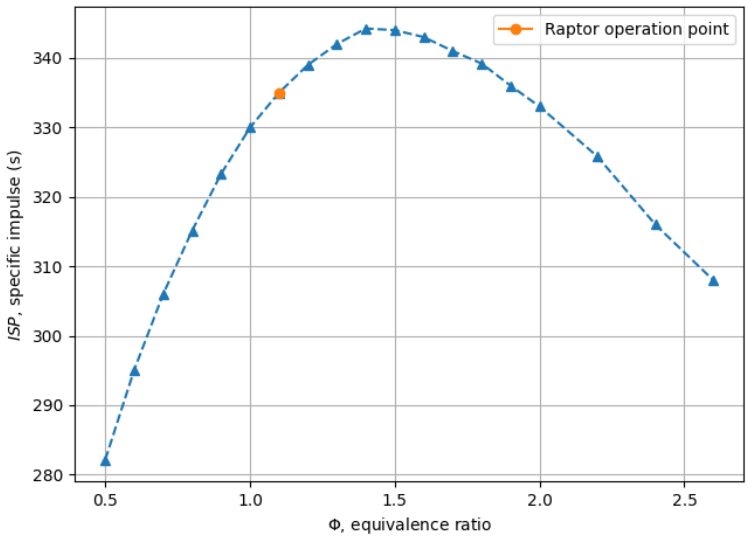

FIGURE 29 Evolution of specific impulse (ISP) versus equivalence ratio Φ

The maximum temperature is reached for stoichiometric combustion when the equivalence ratio (Φ) equals 1. Given that the Raptor engine operates very close to stoichiometric conditions, it experiences very high temperatures. The maximum specific impulse, occurring at Φ = 1.4, reaches 344s, representing a 5.3% increase compared to the Raptor engine's operational point. At this equivalence ratio, maximum temperature within the combustion chamber is decreased of 6.4 %. Consequently, to reduce thermal stress on the rocket engine's combustion chamber and optimize efficiency, it is recommended that the Raptor engine operates at Φ = 1.4. However, this adjustment leads to a 5% increase in pressure within the combustion chamber. We can thus hypothesize that pressure in the combustion chamber serves as the limiting factor in the rocket optimization process.

6 | CONCLUSIONS

In this study, a numerical model has been developed to determine the pressure, temperature, and velocity distribution in the combustion chamber region and the convergent–divergent nozzle of Raptor engine. nozzle. After analyzing the results obtained through simulation, some important conclusions have been made and listed as under:

- The methodology developed (2D, axi-symmetric, and non-premixed combustion) yields a commendable level of accuracy in predicting engine performances.
- The inclusion of preburners within the model significantly enhances the accuracy of engine performance predictions.
- It has been observed that optimization of engine performances can be achieved by varying the equivalence ratio Φ. Notably, our investigations suggest that the pressure within the combustion chamber serves as a limiting factor in the optimization process.

References

[1] SpaceX; 2024. https://www.spacex.com/vehicles/starship/.

[2] Beardslee J. Exhaust Plume Calculations for SpaceX Raptor Booster Engine 2019;.

[3] Wikimedia Foundation; 2024. https://en.wikipedia.org/wiki/SpaceX_Raptor.

[4] Bowman CT. GRI-Mech 2.11 detailed mechanism. University of Berkeley 2024;http://combustion.berkeley.edu/gri-mech/.

[5] Nasa SpaceFlight;. https://www.nasaspaceflight.com/.

[6] Monnier F. Modélisation et simulation numérique de la combustion dans les moteurs-fusées: étude des flammes LOx/CH. PhD thesis, Normandie Université; 2023.

[7] Sharma A, De A, Kumar SS. Numerical investigation of supercritical combustion dynamics in a multi-element LOx–methane combustor using flamelet-generated manifold approach. Physics of Fluids 2023;35(11). http://dx.doi.org/10.1063/5.0172100.

[8] Zubanov V, Egorychev V, Shabliy L. Design of Rocket Engine for Spacecraft Using CFD-Modeling. Procedia Engineering 2015;104:29–35. https://www.sciencedirect.com/science/article/pii/S1877705815007675, scientific and Technological Experiments on Automatic Space Vehicles and Small Satellites.

[9] Bhaskar A, Sahu MK. Numerical investigation on performance of convergent–divergent nozzle with multi-inlet combustion chamber of a rocket engine. Heat Transfer 2022;51(1):5–21. https://onlinelibrary.wiley.com/doi/abs/10.1002/htj.22296.